An efficient, repetitive nanosecond pulsed power generator with ten synchronized spark gap switches

An Efficient, Repetitive Nanosecond Pulsed Power Generator with Ten Synchronized Spark Gap Switches

Z. Liu, A. J. M. Pemen, R. T. W. J. van Hoppe, G. J. J. Winands, E. J. M. van Heesch
Department of electrical Engineering, Eindhoven University of Technology,
P.O.Box 513, 5600 MB Eindhoven, The Netherlands

and **K. Yan**
Department of Environmental Science, Zhejiang University, Hangzhou 310028, China

ABSTRACT

This paper describes an efficient, repetitive nanosecond pulsed power generator using a Transmission-Line-Transformer (TLT) based multiple-switch technology. Within this setup, a 10-stage TLT and ten high-pressure spark-gap switches are adopted. At the input side, ten spark-gap switches are interconnected in series via the TLT, so that all the spark-gap switches can be synchronized automatically. At the output side, all the stages of the TLT are connected in parallel, thus a low output impedance (5 Ω) is obtained, and a large output current is realized by adding the currents through all the switches. Experimental results show that 10 spark-gap switches can be synchronized within about 10 ns. The system has been successfully demonstrated at repetition rates up to 300 pps (Pulses Per Second). Pulses with a rise-time of about 11 ns, a pulse width of about 55 ns, an energy of 9-24 J per pulse, a peak power of 300-810 MW, a peak voltage of 40-77 kV, and a peak current of 6-11 kA have been achieved with an energy conversion efficiency of 93-98%.

Index Terms — **Repetitive pulsed power, multiple switching, spark gaps, transmission line, corona, plasma.**

1 INTRODUCTION

REPETITIVE pulsed power techniques are under investigation for a wide range of applications. Now hundreds of possibilities can be anticipated [1-3]. In particular, repetitive pulsed power supplies have enormous potential in areas such as gas and water processing [4], sterilization [5], intense short-wavelength UV sources [6], high-power acoustics [7], nanoparticle processing [8], etc. Successful introduction of pulsed power in industries depends to a great extent on the availability of highly efficient and reliable cost-effective sources.

The switch is the most critical component for a pulsed power supply. It plays an important role in the performance of a system, affecting factors such as rise-time, efficiency, repetition rate, lifetime, cost, etc. Available switches for systems with capacitive energy storage, which are primarily used, include: semiconductor switches (MOSFET/IGBT), magnetic switches, spark-gap switches, etc. Semiconductor switches have a long lifetime and a high repetition rate (hundreds of kHz or even MHz) [9-11]; the main problems are their limited capacity and high cost for large-scale applications. Magnetic switches are robust and can be also used for high repetition rates (several kHz), however, their energy conversion efficiency for short pulse generation is relatively low (typically 60-80%) [12-16], and there is always a primary switch needed. The spark gap switch can hold a high voltage and carry a large current, and has a low conductive impedance and is easy to construct as well. It is one of the most efficient and cost-effective switches for large pulsed power generation, while its limitation is the lifetime.

Several magnetic-switches based high-power repetitive nanosecond sources were reported. A system described by Mok et al [14], can deliver a ~500 ns (FWHM-full wave at half maximum) pulse with a peak power of ~500 MW, a peak current of 3.3 kA, a rise time of about 200 ns, and a maximal efficiency of 76%. A system described by Lee et al [16], can generate 700 ns pulse with a peak power of ~600 MW, a peak current of ~5 kA, a rise-time of about 70 ns, and a typical energy efficiency of 64.3%. Our previously developed single spark-gap switch based pulse generators are able to produce short pulses (50-100 ns) with a maximal efficiency of 95%, but at a low peak power [17, 18]. In this article, we present a pulsed power generator which can produce efficiently fast rising nanosecond pulses at a relatively high power and a high repetition rate. Experiments were carried out with a resistive load. Pulses with a rise-time of about 11 ns, a pulse width of about 55 ns (FWHM), a peak power of 300-810 MW, and a peak current of 6-11 kA have been obtained with an energy conversion efficiency of 93-98%, and at a repetition rate up to 300 pps.

Manuscript received on 4 July 2008, in final form 7 October 2008.

2 PRINCIPLE

Figure 1 gives a two-switch concept of the topology used in the presented high-power generator [19]. At the input side of the TLT, two identical capacitors C_1 and C_2 are interconnected to the TLT via two switches S_1 and S_2. At the output side, all stages of the TLT are put in parallel to produce a large current. The TLT is made from coaxial cables. Magnetic cores are placed around the cables to increase the secondary mode impedance Z_s, which is defined as the wave impedance between two adjacent stages of the TLT.

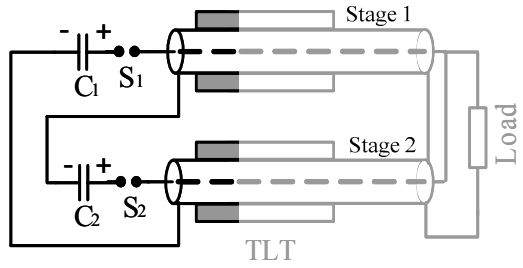

Figure 1. A concept with two switches and a 2-stage TLT.

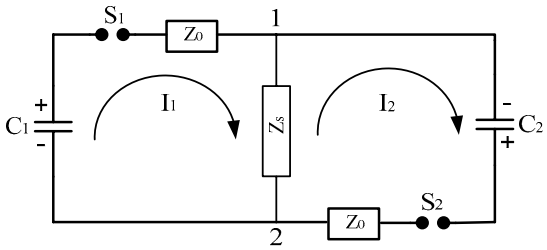

Figure 2. Equivalent circuit at the input side of the TLT.

To gain insight into the principle, an equivalent circuit model shown in Figure 2 can be used [19]. It is derived under the assumption that the TLT is ideally matched at the output side and the transit time for a pulse propagating along the outsides of the TLT is much longer than the time required for the synchronization process of two switches. Here each stage is represented by its characteristic impedance Z_0. Following the connections in Figure 1, it can be seen that both stages (i.e. C_1-S_1-Z_0 and C_2-S_2-Z_0) are connected in series. The secondary mode impedance is represented by Z_s.

Initially, two identical capacitors C_1 and C_2 are charged in parallel up to V_0. Whenever one switch (e.g. S_1) is closed and the other one is still open, a voltage V_{12} will be generated over the secondary mode impedance Z_s, which is equal to $[Z_s/(Z_0+Z_s)]\times V_0$. Because the Z_s is designed to be much larger than the characteristic impedance Z_0 of the TLT, the discharging of capacitor C_1 or C_2 is prevented, and the value of V_{12} could be up to V_0. Moreover, because the stray capacitance of the spark gap switch S_1 or S_2 is much smaller than the capacitance of C_1 or C_2, the voltage across the unclosed switch can rise from V_0 up to $V_0+V_{12}\approx 2V_0$. This generated overvoltage will force the second switch to close subsequently.

When all the switches are closed, one can derive the following equations from the equivalent circuit in Figure 2:

$$\begin{cases} I_1(t)\cdot(Z_0+Z_s)-I_2(t)\cdot Z_s = V_0-\dfrac{1}{C_0}\displaystyle\int_0^t I_1(\tau)d\tau \\ I_2(t)\cdot(Z_0+Z_s)-I_1(t)\cdot Z_s = V_0-\dfrac{1}{C_0}\displaystyle\int_0^t I_2(\tau)d\tau \end{cases} \quad (1)$$

In above equations, $I_1(t)$ and $I_2(t)$ are the currents through switches S_1 and S_2 respectively, and C_0 is the value of capacitors C_1 and C_2 (C_1 and C_2 are identical). Solving these two equations, one can obtain the following expressions for $I_1(t)$ and $I_2(t)$:

$$I_1(t) = I_2(t) = \frac{V_0}{Z_0}\cdot\exp\left(\frac{-t}{Z_0\cdot C_0}\right) \quad (2)$$

It can be seen that after both switches are closed, the switching currents $I_1(t)$ and $I_2(t)$ are identical. The voltage V_{12} across Z_s will drop to zero. Now all stages of the TLT are used in parallel equivalently. After a short time delay (transit time of the TLT), a pulse will be generated over the loads at the output side. The output current is twice the switching current in the circuit as shown in Figure 1.

It is noted that for a practical circuit, although the described model cannot be used to accurately derive the switching behaviors due to the limited secondary mode impedance Z_s and the finite length of the TLT, it presents the basic principle of the technology. In principle, the circuit topology described in Figure 1 can be extended for a number of switches for high power generation. Moreover, except the parallel configuration, at the output side, the TLT can be put in series for high-voltage generation, or can be used to drive independent loads simultaneously [19].

3 DEVELOPMENT OF AN EFFICIENT HIGH-POWER PULSE GENERATOR

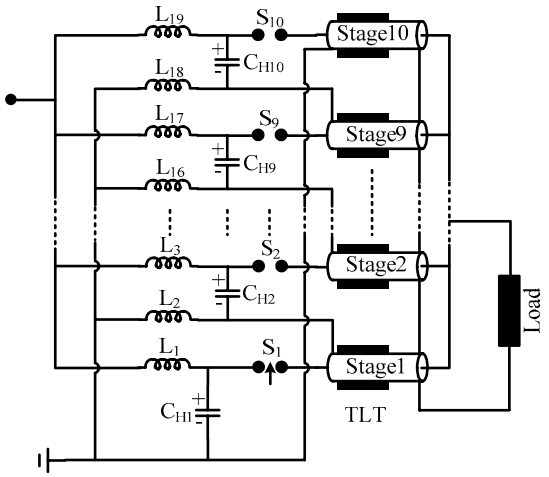

Figure 3. The main circuit of the high-power generator.

The main circuit of the generator is shown in Figure 3. It includes 19 charging inductors, 10 high-voltage capacitors, ten spark-gap switches, a ten-stage TLT with one single cable per stage. At the input side, the switches are interconnected

via the TLT. At the output side, all the stages of the TLT are connected in parallel, thus the output impedance is very low (5 Ω). The ten switches are high-pressure spark gap switches. One of them is a triggered switch, while the others are self-breakdown switches. The TLT is made from coaxial cable (RG218, Z_0=50 Ω) and each stage is 2 m long. The circuit in Figure 3 is connected the same way as in Figure 1. Now the current is reduced by a factor of 10 in each of the switches, in comparison to a single-switch setup. The lifetime is expected to improve significantly. For the detailed discussion about the lifetime, please see Section 5.

3.1 CHARGING INDUCTORS

The nineteen inductors L_1-L_{19}, shown in Figure 3, are used to charge the high-voltage capacitors C_{H1}-C_{H10} in parallel. While during the synchronization process of the ten spark-gap switches, they also provide high impedance to prevent the discharging of the high-voltage capacitors. To ensure proper synchronization, the value L of the inductors must be:

$$L >> \frac{Z_s \cdot \Delta T_s}{2} \quad (3)$$

where ΔT_s is the time interval for the synchronization of all switches. For instance, when Z_s=2 kΩ and ΔT_s=30 ns, the inductance should be much larger than 30 μH. Within the present setup, air-core inductors were used. They are made from the copper wire with a diameter of 1.06 mm wound on a plastic cylinder, as shown in Figure 4. The inductance value of each inductor was measured to be 605 μH.

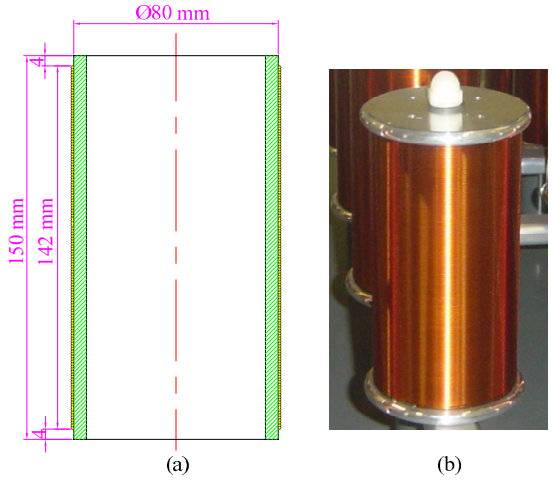

Figure 4. (a) Sketch of the inductor, (b) photo of the inductor.

3.2 SPARK GAP SWITCHES

High-pressure spark-gap switches (S_1-S_{10}) were used for the present system. Compared with atmospheric-pressure spark gaps, the advantages of a high-pressure spark gap are: (i) smaller conductive resistance, (ii) smaller inductance, and (iii) a faster switching time due to the shorter gap distance and higher field strength. For a uniform or nearly uniform gap filled with air, the breakdown voltage V_B is a function of the air pressure p and the gap distance d, and can be expressed as:

$$V_B = 24.4pd + 6.7\sqrt{pd} \quad (4)$$

where p and d are the air pressure in bar and the gap distance in cm respectively [20].

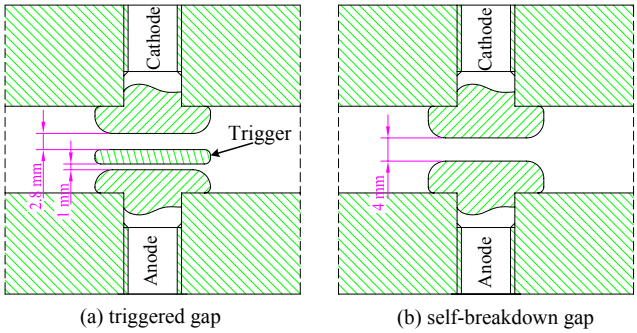

Figure 5. Sketch of the spark gaps.

Brass was chosen as the electrode material, since this material is cheap and easy to machine. Also the electrode erosion rate is low according to the result found in literatures [21, 22]. If necessary, brass can be easily replaced by other materials. The diameter of each electrode is 20 mm. Figure 5 shows the sketches of the triggered switch (S_1) and the self-breakdown switches. They were designed to have the same breakdown voltage in accordance with equation (4). For the self-breakdown switches, the gap distance is 4 mm. For the triggered switch, the distances of the trigger gap and the gap between the trigger electrode and the cathode are 1 mm and 2.8 mm respectively.

3.3 THE TLT

The TLT plays an important role in synchronizing the multiple switches and in transferring the energy from the capacitors to the load [19]. To ensure the synchronization and to prevent the discharging of the high-voltage capacitors during the synchronization process, the secondary mode impedance Z_s of the TLT must be much larger than the characteristic impedance Z_0 of the coaxial lines, namely:

$$Z_s >> Z_0 \quad (5)$$

Moreover, to avoid reflections of the high-voltage pulse between the outer conductors of the TLT, the transit time between the outer conductors of the TLT should be longer than $\Delta T_s/2$. Therefore, the length l of the coaxial cables covered by magnetic cores needs to be:

$$\frac{l}{\upsilon_s} \geq \frac{1}{2}\Delta T_s \quad (6)$$

In the above equation, υ_s is the wave velocity between the outer conductors of the TLT.

During the synchronization process, the overvoltage induced by the closing of the first switch is shared by the rest switches that are not closed yet. When a large number of switches are used, the overvoltage may be too small to close the second switch. This may cause the failure of the synchronization. To obtain proper synchronization, different secondary mode impedances of the TLT are desirable. By this way, the overvoltage induced by the closing of the first switch will be nonuniformly added to the unclosed switches. The switch with more overvoltage will close shortly after the closing of switch S_1. Once one switch can be closed shortly after the first switch, the synchronization can be accomplished properly. Within the present system, the same magnetic cores are placed around the specific stages of the TLT, as shown in

Figure 6. Magnetic cores are not put around the cables of stages nos. 3, 6 and 8. The secondary mode impedances between two adjacent stages covered or not covered by magnetic cores are different. After the closing of the switch S_1, the switches S_2, S_5 and S_{10} have the highest voltage, which is theoretically about $1.14V_0$ (V_0 is the charging voltage). By means of the configuration as shown in Figure 6, proper synchronization has been realized. Actually, instead of stages 3, 6, and 8, one may also choose another set (e.g. 3, 5 and 7). But note that (1) stages 1 and 10 must be covered to prevent the discharging of C_{H1} because S_1 is triggered firstly and the secondary impedance formed by stages 1 and 10 sees the high voltage during the whole synchronization process; (2) at least one out of adjacent stages is covered to form a high secondary mode impedance.

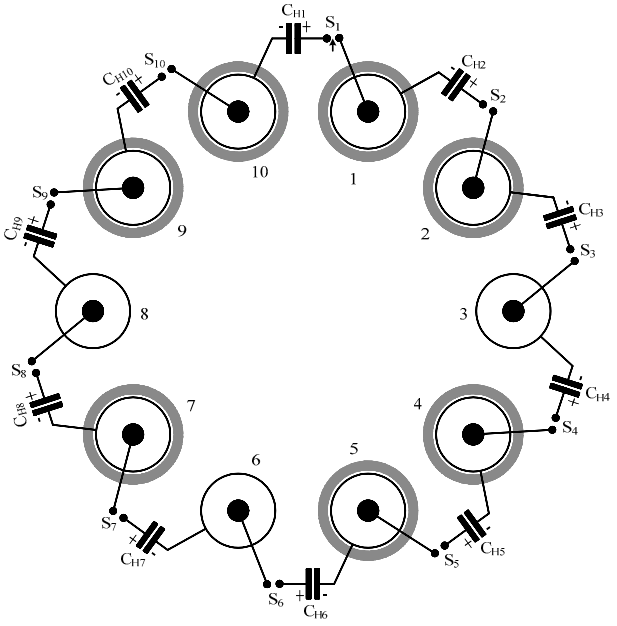

Figure 6. Configuration of the magnetic cores around the coaxial cables of the TLT.

Figure 7. Schematic diagram of two parallel coaxial cables covered with magnetic material.

In addition, to obtain a high secondary mode impedance, saturation of the magnetic material must be avoided. Thus equation (7) must be met:

$$B_s > \frac{\mu_0 \mu_r V_p}{\ell_m Z_s} \tag{7}$$

where B_s is the saturation flux density of the magnetic material, ℓ_m is the mean length of the magnetic path of the magnetic toroid, and V_p is the voltage over the secondary mode impedance Z_s.

To evaluate the effect of the magnetic material used in the TLT, the model shown in Figure 7 can be used. Here D is the distance between the magnetic cores, D_0 is the diameter of the outer conductor of the coaxial cables of the TLT, D_1 and D_2 are the inner and outer diameters of the magnetic toroid respectively. The secondary mode impedance and wave velocity can be estimated by:

$$Z_{2s} = 120\sqrt{\{\ln\frac{2D+D_0}{D_0} + (\mu_r - 1)[\ln\frac{D_2}{D_2} + \ln\frac{2(D+D_0)-D_1}{2(D+D_0)-D_2}]\}\ln\frac{2D+D_0}{D_0}} \tag{8}$$

$$Z_{1s} = 120\sqrt{\{\ln\frac{2D+D_0}{D_0} + \frac{1}{2}(\mu_r - 1)[\ln\frac{D_2}{D_2} + \ln\frac{2(D+D_0)-D_1}{2(D+D_0)-D_2}]\}\ln\frac{2D+D_0}{D_0}} \tag{9}$$

$$\upsilon_{2s} = \upsilon_0\sqrt{\{\ln\frac{2D+D_0}{D_0} + (\mu_r - 1)[\ln\frac{D_2}{D_2} + \ln\frac{2(D+D_0)-D_1}{2(D+D_0)-D_2}]\}^{-1}\ln\frac{2D+D_0}{D_0}} \tag{10}$$

$$\upsilon_{1s} = \upsilon_0\sqrt{\{\ln\frac{2D+D_0}{D_0} + \frac{1}{2}(\mu_r - 1)[\ln\frac{D_2}{D_2} + \ln\frac{2(D+D_0)-D_1}{2(D+D_0)-D_2}]\}^{-1}\ln\frac{2D+D_0}{D_0}} \tag{11}$$

In the equations shown above, Z_{2s} and υ_{2s} are the secondary mode impedance and the wave velocity when magnetic cores are placed around both coaxial cables. Similarly, Z_{1s} and υ_{1s} are for the situation when only one coaxial cable is covered with magnetic cores. μ_r is the relative permeability of the magnetic material. υ_0 is the wave velocity in air. This model was proven for the case of a two-stage TLT previously [23].

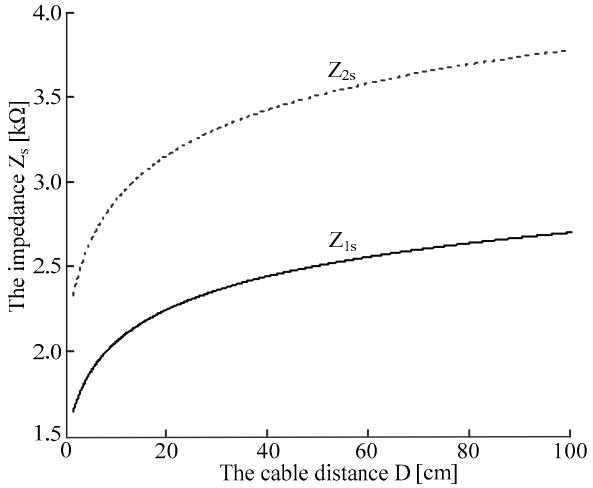

Figure 8. Calculated secondary mode impedance Z_{1s} and Z_{2s} versus D based on equations (8) and (9).

The magnetic material used within the present setup is metglass MP4510. Its relative permeability μ_r is 245. The values of D_0, D_1 and D_2 are 18.3 mm, 19.6 mm, and 48.4 mm respectively. Calculated values of the secondary mode impedance and the wave velocity versus distance D are shown in Figures 8 and 9 respectively. It can be seen that a secondary mode impedance Z_s>2 kΩ can be obtained. Upon increasing the value of D from 10 cm to 100 cm, the ratio of Z_{2s} to Z_{1s} is 1.4. For a value of D less than 100 cm, the values of υ_{2s} and υ_{1s} are less than 4.47×10^7 m/s and 6.25×10^7 m/s respectively. If the length covered by magnetic material is 100 cm, the two-way transit times corresponding to υ_{2s} and υ_{1s} are 45 ns and 32 ns respectively. In addition, the values of B_s and ℓ_m of metglass MP4510 are 1.56 T and 10.55 cm respectively. The

magnetic material is used far below the saturation, for instance, when Z_s =2 kΩ and V_p=40 kV the flux density inside the toroid is only 0.058 T.

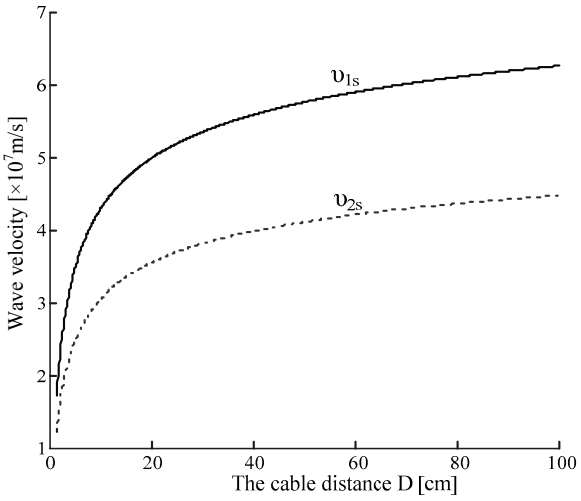

Figure 9. Calculated wave velocity υ_{1s} and υ_{2s} versus D based on equations (10) and (11).

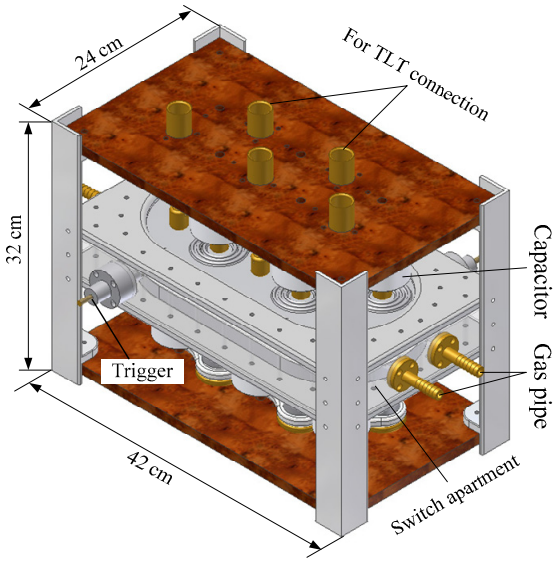

(a) 3-D overview

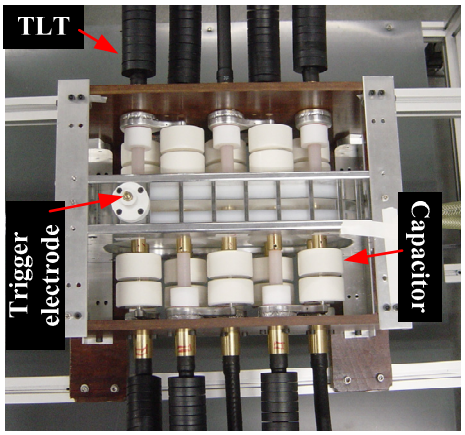

(b) Side view

Figure 10. The compact design at the input side of the TLT.

3.4 THE COMPACT CONSTRUCTION

To obtain a fast high-power pulse, the setup must be as compact as possible. Within the present work, the ten switches S_1-S_{10}, the ten high-voltage capacitors C_{H1}-C_{H10}, and the input side of the TLT are integrated into one compact structure, as shown in Figure 10. The ten switches are installed in one single compartment. Consequently, they "see" each other's UV and other discharge products, which will also help the synchronization process. The ten switches are put into two arrays, with five switches per array. A compressed air flow is used to flush the spark gap switches for the high-voltage and high-repetition-rate operation. This unit is able to hold a pressure up to 1 MPa (10 bar).

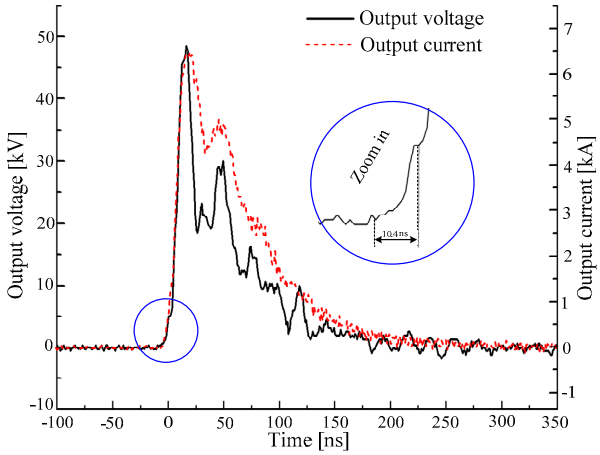

Figure 11. Typical output voltage and current (the rise-time of the output voltage and current are 11.0 ns and 12.2 ns respectively).

4 THE OUTPUT CHARACTERISTICS

With a forced air cooling of the load, this setup has been demonstrated at a repetition rate from 10 to 300 pps, and no synchronization error occurred. Figure 11 shows typical waveforms of output voltage and current when the setup was connected to a matched resistive load of 5 Ω, and operated at a repetition rate of 20 pps. For the ten-switch compartment, the input and output pressure were 0.34 MPa (3.4 bar) and 0.24 MPa (2.4 bar), respectively. The gas flow rate was about 5 Liters per second, and the gas flow velocity was estimated to be approximately 1.8 m/s. The voltage on the high-voltage capacitors when the switches closed was 42.8 kV (switching voltage). The peak values of the output voltage and current are 48.4 kV and 6.46 kA respectively. The rise-times (10-90%) of the output voltage and current are 11.0 ns and 12.2 ns respectively. In addition, it is seen that a small step with a duration of about 10.4 ns occurs within the rising part of the output pulse (see magnified view in Figure 11). This, in fact, implies that the ten spark gap switches are closed in sequence within about 10.4 ns. The peak output power and the output energy for the measurement shown in Figure 11 are 312 MW and 9.31 J, respectively. The voltage on the high-voltage capacitors when the switches closed was 42.8 kV. Therefore, ideally (i.e. no energy loss and the TLT with a perfectly matched load), the value of the peak output power should be 366 MW. Actually, due to the energy losses and the

mismatching, the obtained peak power is 85% of the ideal value.

Figure 12 plots the averaged output current (averaged over 101 shots) and a last single shot record when the setup was operated at 50 pps. We observed that the last pulse in series coincided with the trace of the average in all the tests up to 150 pulses per second. While when the repetition rate was increased up to above 150 pps, it was observed that a difference between these two signals occurred. This indicates that the output becomes unstable at the repetition rate above 150 pps. Possibly the cooling of the load is insufficient to cool it and keep its resistance stable at a high repetition rate. Consequently, the current changes slightly during operation.

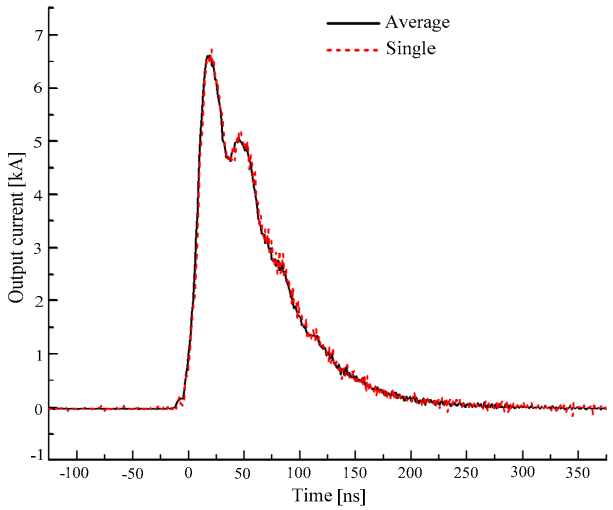

Figure 12. The averaged output current (averaged over 101 shots) and a single shot record.

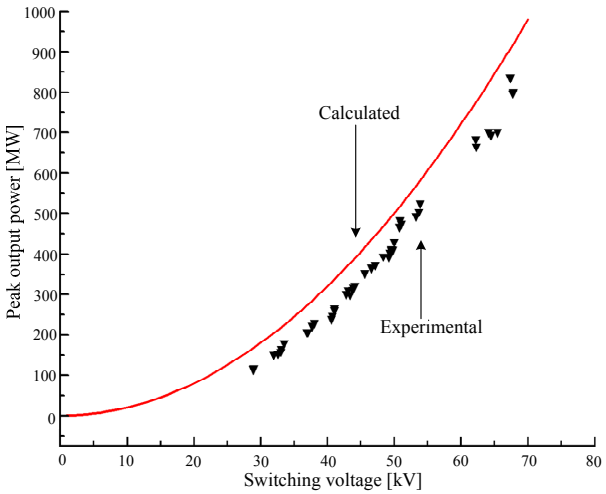

Figure 13. Peak output power at different switching voltages.

Besides the experiments described above, the testing was also carried out with the different switching voltages from 28 kV to 70 kV. The air pressure was adjusted from 0.25 MPa (2.5 bar) to 0.6 MPa (6 bar). The present system works well at different situations. Figure 13 gives the peak output power at different switching voltages. The ideal value of the peak output power is also given in Figure 13, which is calculated under the assumption that the TLT is perfectly matched and the energy loss is neglected. Apparently, due to energy losses and the reflection, the experimental values are always less than those calculated ones. When the setup was operated with a switching voltage of about 70 kV, the peak output power of 810 MW with an output energy of 24.1 J was obtained, as shown in Figure 14. And its peak values of output voltage and current are 76.8 kV and 11.0 kA, respectively.

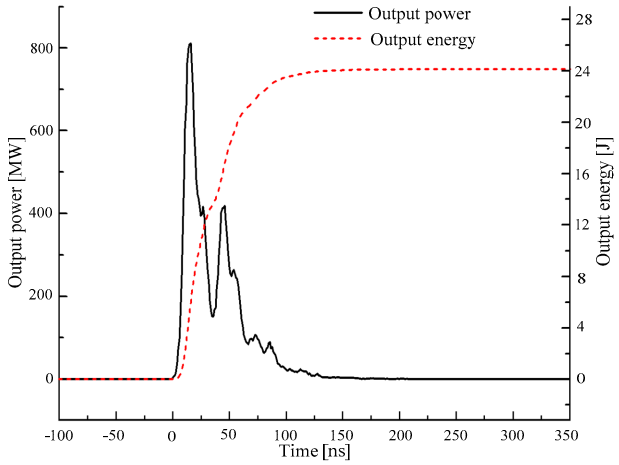

Figure 14. The typical output power and energy at the switching voltage of 69.7 kV (the peak output power and the output energy are 810 MW and 24.1 J respectively).

The energy conversion efficiency of the ten-switch prototype was evaluated for different operation situations according to the following equation.

$$\eta = \frac{E_{load}}{E_{charging}} = \frac{\int V_{output}(t) I_{output}(t) dt}{\int V_H(t) I_H(t) dt} \qquad (12)$$

where, E_{load} and $E_{charging}$ are the energy obtained in the load and the total energy used to charge the setup, respectively. They are calculated by integrating the corresponding product of the voltage and the current. Within the present setup, the energy conversion efficiency is 93-98%. It is observed that the higher the switching voltage, the higher the energy conversion efficiency.

5 Discussion

The electrode erosion is the main factor which limits the lifetime of a spark gap switch. Donaldson et al conducted comprehensive investigations on the electrode erosion [22, 24-25]. They developed a law using a thermal model to scale the electrode erosion rate (i.e. erosion volume per shot) with a typical pulse parameter (e.g. peak current I_p, transferred charge Q_e, factor $F=I_pQ_e\tau^{1/2}$ where τ is the pulse duration, etc.). Over 40 different kinds of electrode materials were tested. According to their observations, the electrode erosion rate exhibits a similar trend as function of pulse parameters [24], as predicted by their scaling law. There exist three different regions [22, 24]: (1) when the typical parameter is

below a certain threshold, the erosion is dominated by the vaporization and increases linearly (in the logarithmic coordinates) with the parameter; (2) when the parameter is above a certain value, the erosion is dominated by the ablation and has the same dependence on the parameter as in region (1), but with one order higher magnitude; (3) there is a narrow transient area between (1) and (2); in this region the erosion increases fast from the first regime to the second regime. From their findings, one can see that the erosion rate will decrease when the parameter decreases, no matter which regime is considered. In our situation, the total switching current is shared by ten switches, and the current is reduced by a factor of 10 in each of them. Based on Donaldson et al, the erosion rate in each switch will be reduced in comparison to a single-switch setup. To estimate that how much can be gained in life-time, it is convenient to use the F factor. With this factor, they succeeded in fitting the results from different experiments [25]. On both sides of the transient region (3) the erosion rate increases linearly with F. For the ten-switch setup, the current is reduced by a factor of ten in each switch, which means that the F value is reduced by a factor of 100. Therefore, the erosion rate is expected to be reduced by a factor of about 100. In comparison to a single-switch setup with the same power level, the lifetime of the ten-switch setup is expected to improve by a factor of about 100 if the erosion distribution over the surface of the electrode remains unaltered.

In future, the setup could be made more compact. Since the synchronization process is completed within about 10 ns (experimental result) instead of the safe design value of 30 ns, shorter cables can be used. The length covered by magnetic cores can be shorter. The volume occupied by the switch unit, the TLT and the output could be 30×40×100 cm^3. The volume occupied by the charging inductors is quite large. Replacing the capacitors with cables or using a multiple-switch Blumlein topology [26], the charging inductors can be eliminated.

6 CONCLUSION

Through use of the TLT based multiple-switch circuit topology, repetitive nanosecond high-power (up to about 1 GW) pulse source with a fast rise-time (11 ns) is achievable. The development of the ten-switch setup was described, and the experimental results were discussed. The setup has been operated properly at repetition rates up to 300 pps. Ten switches can be synchronized within about 10 ns. This system is able to produce pulses with a rise-time of about 11 ns and a width of about 55 ns. The peak output power of over 800 MW with a peak output current of about 11 kA was obtained. The energy conversion efficiency is 93-98%. High volume-density corona plasma generation by using this system is under investigation, and results will be reported in future.

ACKNOWLEDGMENT

The presented work is funded by the Dutch IOP/EMVT program. Sincere thanks go to Mr. Ad van Iersel for the help on experiments.

REFERENCES

[1] S. Levy, M. Nikolich, I. Alexeff, M. T. Buttram, and W. J. Sarieant, "Commercial applications for modulators and pulse power technology", 20th Power Modulator Sympos., pp. 8-14, 1992.

[2] M. Kristiansen. "Pulsed power applications", 9th IEEE Intern. Pulsed Power Conf., pp. 6-10, 1993.

[3] H. Bluhm, *Pulsed Power Systems, Springer*, 2006.

[4] E. M. van Veldhuizen, *Electrical Discharges for Environmental Purposes: Fundamentals and Applications*, New York: Nova Science Publishers, 2000.

[5] H. H. Kim, "Nonthermal plasma processing for air-pollution control: A historical review, current issues and future prospects", Plasma Process. Polym,. Vol. 1, No. 2, pp. 91-110, 2004.

[6] E. R. Kieft, *Transient Behavior of EUV Emitting Discharge Plasmas a Study by Optical Methods,* PhD dissertation, Eindhoven University of Technology (http://alexandria.tue.nl/extra2/200512577.pdf).

[7] E. J. M. van Heesch, K. Yan, A. J. M. Pemen, S. A. Nair, G. J. J. Winands, and I. de Jong, "Matching repetitive pulsed power to industrial processes", IEEJ Trans. Fundamentals Materials, Vol. 124, pp. 607-612, 2004.

[8] K. Ostrikov, "Reactive plasmas as a versatile nanofabrication tool", Rev. Modern Phys., Vol. 77, pp. 489-511, 2005.

[9] J. A. Watson, E. G. Cook, Y. J. Chen, R. M. Anaya, B. S. Lee, J. S. Sullivan, S. A. Hawkins, F. V. Allen, B. C. Hickman, and C.A. Brooksby, "A solid-state modulator for high speed kickers", Intern. Particle Accelerator Conf., pp. 3738-3740, 2001.

[10] W. Jiang, T. Matsuda, and K. Yatsui, "MHz pulsed power generator using MOS-FET", 25th Intern. Power Modulator Sympos., pp. 599-601, 2002.

[11] Y. Kotlyar, W. Eng, C. Pai, J. Sandberg, J. Tuozzolo, and W. Zhang, "Principle design of 300 kHz MECO RF kicker bipolar solid state modulator", 26th Intern. Power Modulator Sympos., pp. 250-253, 2004.

[12] W. Jiang, T. Matsuda, and K. Yatsui, "High repetition-rate, low jitter pulsed power generator for excimer laser applications", 25th Power Modulator Sympos., pp. 605-607, 2002.

[13] H. M. von Bergmann, and P. H. Swart, "Thyristor-driven pulsers for multikilowatt average power lasers", Electric Power Applications, Vol. 139, No. 2, pp. 123-130, 1992.

[14] Y. S. Mok, H. W. Lee, and Y. J. Hyun, "Flue gas treatment using pulsed corona discharge generated by magnetic pulse compression modulator", J. Electrostatics, Vol. 53, pp. 195-208, 2001.

[15] G. H. Rim, B. D. Min, E. Pavlov, and J. H. Kim, "Repetitive nanosecond all-solid-state pulse generator using magnetic switch and SOS diodes", IEEE Pulsed Power Conf., pp. 1069-1072, 2005.

[16] Y. H. Lee, W. S. Jung, Y. R. Choi, J. S. Oh, M. S. D. Jang, Y. G. Son, M. H. Cho, W. Namkung, D. J. Hoh, Y. S. Mok, and J. W. Chung, "Application of pulsed corona induced plasma chemical process to an industrial incinerator", Environ. Sci. Technol., Vol. 37, pp. 2563-2567, 2003.

[17] K. Yan, E. J. M van Heesch, A. J. M. Pemen, P. A. H. J. Huijbrechts, and P. C. T. Van der Laan, "A 10 kW high-voltage pulse generator for corona plasma generation", Rev. Sci. Instrum., Vol. 72, pp. 2443-2447, 2001.

[18] G. J. J. Winands, K. Yan, A. J. M. Pemen, S. A. Nair, Z. Liu, and E. J. M. van Heesch, "An industrial streamer corona plasma system for gas cleaning", IEEE Trans. Plasma Sci., Vol. 34, pp. 2426-2433, 2006.

[19] Z. Liu, K. Yan, A. J. M. Pemen, G. J. J. Winands, and E. J. M. Van Heesch, "Synchronization of multiple spark-gap switches by a transmission line transformer", Rev. Sci. Instruments, Vol. 76, Issue 11, (113507) 2005.

[20] E. Kuffel, and W. S. Zaengl, *High Voltage Engineering - Fundamentals*. ISBN 0-08-024213-8, Pergamon Press, 1984.

[21] J. M. Koutsoubis, and S. J. MacGregor, "Electrode erosion and lifetime performance of a high repetition rate, triggered, corona-stabilized switch in air", J. Phys. D: Appl. Phys., Vol. 33, pp. 1093-1103, 2000.

[22] A. L. Donaldson, T. G. Engel, and M. Kristiansen, "State-of-the-art insulator and electrode materials for use in high current high energy switching", IEEE Trans. Magnetics, Vol. 25, pp. 138-141, 1989.

[23] G. J. J. Winands, *Efficient Streamer Plasma Generation*, Ph.D. dissertation., Eindhoven University of Technology, the Netherlamds, ISBN-978-90-386-1040-5, 2007.

[24] A. L. Donaldson and M. Kristiansen, "Utilization of a thermal model to predict electrode erosion parameters of engineering importance", 19th IEEE intern. Power Modulator Sympos., pp.265-269, 1990.
[25] F. M. Lehr, and M. Kristiansen, "Electrode erosion from high current moving arcs", IEEE Trans. Plasma Science, Vol. 17, No. 5, pp. 811-817, 1989.
[26] Z. Liu, K. Yan, G. J. J. Winands, E. J. M. Van Heesch, and A. J. M. Pemen, "Novel multiple-switch Blumlein generator", Rev. Sci. Instruments, Vol. 77, Issue 03, (033502) 2006.

Zhen Liu was born in Xiang Cheng, China in 1978. He received the B.Sc. degree from Xi'an Jiaotong Univerisity, Xi'an, China in 2000, the M.Sc. degree from Tsinghua University, Beijing, China in 2003 and the Ph.D. degree at the Electrical Power Systems Group (EPS), Technische Universiteit Eindhoven (TU/e), The Netherlands in 2008. Currently he is with EPS group as a Postdoc researcher. His research interest includes pulsed power generation, plasma and applications.

A. J. M. Pemen (M'98) received the B.Sc. degree from the College of Advanced Technology, Breda, The Netherlands, in 1986 and the Ph.D. degree in electrical engineering from the Eindhoven University of Technology, The Netherlands, in 2000, both in electrical engineering. Before joining the Electrical Power Systems Group (EPS), Eindhoven University of Technology in 1998 as an Assistant Professor, he was with KEMA T&D Power, Arnhem, The Netherlands. He is currently involved in research on pulsed-power and pulsed plasma. His research interest includes high-voltage engineering, pulsed-power, plasmas, and renewable energy systems. Among his achievements are the development of an on-line monitoring system for partial discharges in turbine generators, a pulsed-corona system for industrial applications, and a pulsed corona tar cracker. He is the Founder of the Dutch Generator Expertise-Center.

R. T. W. J. van Hoppe joined the Electrical Power System (EPS) group, Technische Universiteit Eindhoven (TU/e), The Netherlands in 2001. Currently, he is responsible as a lectuerer/instructor for some courses, and also involved in a student educational project as an expert. Moreover, he is involved in research projects in the EPS group, giving guidance for graduate student and support for Phd candidates.

G. J. J. Winands was born in Kerkrade, The Netherlands, in 1978. He received the M.Sc. degree in applied physics from the Eindhoven University of Technology, The Netherlands, in 2002, and the Ph.D. degree at the faculty of Electrical Enginnering of the same university in 2007. Currently he works on industrial pulsed corona systems for air treatment at HMVT, Ede, The Netherlands. His activities focus on the interaction between power modulator and plasma generation/chemical processing, and are related to repetitive plasma generation for industrial scale gas-cleaning applications.

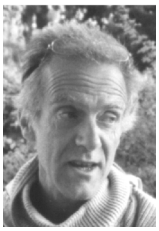

E. J. M. van Heesch was born in Utrecht, The Netherlands, in 1951. He received the Master's degree in physics from the Eindhoven University of Technology, The Netherlands, and the Ph.D. degree in plasma physics and fusion related research from the University of Utrecht, The Netherlands, in 1975 and 1982, respectively. Since 1986, he has been an Assistant Professor at the Eindhoven University of Technology. Here, he is leading pulsed-power research. He was previously involved with shock-tube gas dynamics (Eindhoven, 1975) and with fusion technology (Jutphaas, The Netherlands, 1975–1984, Suchumi former USSR, 1978 and Saskatoon, Canada, 1984–1986). Among his designs are various plasma diagnostics, a toroidal fusion experiment, substation high-voltage measuring systems and systems for pulsed-power processing. He organizes many projects with industry and national and European Union research agencies. His research is the basis for teaching and coaching university students and Ph.D. candidates. He is a co-inventor of several patents and has coauthored more than 100 publications.

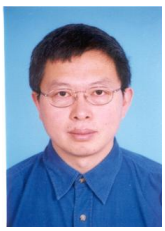

Keping Yan received the B.S. and M.S. degrees in applied physics from Beijing Institute of Technology, Beijing, China, and the Ph.D. degree, which focused on corona plasma generation, from Eindhoven University of Technology, Eindhoven, The Netherlands, in 1983, 1986, and 2001, respectively. In 2006, he joined the Department of Environmental Science, Zhejiang University, Hangzhou, China, as a Full Professor. In 2004, he became a Board Member of the International Society for Electrostatic Precipitation. He is the coauthor of approximately 40 papers in journals and the holder of ten patents. Since 1988, his research interests have included applied plasma technology, corona applications, and pulsed-power sources.